ADVANCED FUNCTIONAL MATERIALS
www.afm-journal.de

Visibly Clear Radiative Cooling Metamaterials for Enhanced Thermal Management in Solar Cells and Windows

*Kang Won Lee, Woojong Lim, Min Soo Jeon, Hanmin Jang, Jehwan Hwang, Chi Hwan Lee, and Dong Rip Kim**

The study of transparent daytime radiative cooling with no additional energy consumption is a promising area of research. Its applications include solar cells and building and automobile windows that are prone to heating issues. Ubiquitous applications necessitate the development of metamaterials with high mechanical flexibility in a scalable manner while overcoming translucence. In this study, visibly clear and flexible radiative cooling metamaterials have been developed using a newly designed optical modulator filled into randomly distributed silica aerogel microparticles in a silicone elastomer. The optical modulator effectively suppresses visible light scattering, thus enabling higher loading of silica aerogel microparticles while securing visible clarity. The significant suppression of the rise in temperature by the metamaterial is verified using both indoor and outdoor experiments. The visibly clear metamaterials deployed in solar cells and windows can effectively suppress the rise in temperature under solar irradiation, thereby mitigating the performance degradation of solar cells by heating issues and suppressing the rise in temperature of indoor air.

1. Introduction

Daytime radiative cooling can be achieved by proper optical management of sunlight. In recent years, it has gained popularity owing to its promising features, such as decreasing or maintaining the temperature of a target application, including electronic devices, buildings, and fabrics, when exposed to sunlight without additional energy consumption.[1–5] Effective daytime radiative cooling can be accomplished when the incident sunlight is mostly reflected at wavelengths of 0.3–2.5 μm while dissipating heat toward the outer spaces by increased light emission in the atmospheric window at wavelengths of 8–13 μm.[6] Based on the experimental analysis, it has been observed that diverse photonic structures and metamaterials manipulate the solar reflection and thermal emission for daytime radiative cooling. One of the approaches involves depositing seven layers of hafnium oxide (HfO_2) and silicon oxide (SiO_2) on a silicon wafer. It was observed that the temperature of the target device (e.g., Si wafer) decreased by approximately 4.9 °C, which was below the ambient air temperature, by reflecting 97 % of the incident visible light while achieving strong and selective light emission in the atmospheric window under a solar intensity of approximately 890 W m^{-2} in Stanford, California, USA.[6] Inspired by Saharan silver ants or longicorn beetles, pyramid-shaped polydimethylsiloxane (PDMS) surfaces achieved 95–97 % solar reflection in the solar spectral range with high light emission characteristics of 96–98 % in the atmospheric window, which led to a maximum temperature drop of 5.1–6.2 °C below the ambient air temperature under a solar intensity of approximately 862 W m^{-2} in China.[7,8] The emission/absorption peaks of functional groups of polymers, such as polyvinylidene fluoride (PVDF) and poly(methyl methacrylate) (PMMA), were studied for a better understanding of daytime radiative cooling.[9] In addition, polymer resins (e.g., acrylic resin, polyethylene mixed with nanoparticles (e.g., titanium oxide (TiO_2), polytetrafluoroethylene (PTFE), zinc oxide (ZnO), carbon, silicon carbide (SiC), and SiO_2 nanoparticles)) have been used to realize effective radiative cooling metamaterials.[10–14] Hierarchically structured porous polymer coatings realized by mixing poly(vinylidene fluoride-co-hexafluoropropene) in acetone and water demonstrated excellent visible light reflectance (≈96 %) and light emission (≈97 %) in the atmospheric window, leading to sub-ambient temperature drops of ≈6 °C under a solar intensity of approximately 890 W m^{-2} in Phoenix, Arizona, USA.[15] Nano-micro-structured porous polymer synthesized by liquid-liquid separation between methacrylic acid and water exhibited

K. W. Lee, W. Lim, M. S. Jeon, H. Jang, D. R. Kim
School of Mechanical Engineering
Hanyang University
Seoul 04763, South Korea
E-mail: dongrip@hanyang.ac.kr
J. Hwang, C. H. Lee
Weldon School of Biomedical Engineering
Purdue University
206 S Martin Jischke Dr, West Lafayette, IN 47907, USA
C. H. Lee
School of Mechanical Engineering
Purdue University
585 Purdue Mall, West Lafayette, IN 47907, USA
C. H. Lee
School of Materials Engineering
Purdue University
701 W Stadium Ave, West Lafayette, IN 47907, USA

The ORCID identification number(s) for the author(s) of this article can be found under https://doi.org/10.1002/adfm.202105882.

DOI: 10.1002/adfm.202105882

solar reflectance of ≈96% and light emission (≈90%) in the atmospheric window.[16] Engineered wood with delignification and subsequent mechanical pressing possessed partially aligned cellulose nanofibers that exhibited radiative cooling effects of ≈4 °C below the ambient temperature in 16 cities in the USA.[3] Polyethylene oxide (PEO) film with electrospun nanofibers acted as an excellent thermal selective emitter for high-performance all-day radiative cooling effects.[17]

Despite their advantages, these metamaterials are optically opaque, thus maximizing the reflection of incident sunlight, including the visible wavelengths. The transmission of visible light in metamaterials can impede the realization of sub-ambient temperature drops. Nonetheless, rendering the daytime radiative cooling platform transparent, while significantly suppressing the rise in temperature by solar irradiation, can be beneficial. This feature can be used in many applications, such as solar cells and building and automobile windows, that are prone to heating issues.[1,3,18–20] Recently, transparent radiative cooling materials have been actively studied by implementing light management to transmit visible light while achieving a high degree of light emission in the atmospheric window.[14,19] SiO_2 pyramid arrays were formed on a bare Si substrate, and transparent radiative cooling effects were numerically investigated to achieve cooling effects of approximately 17.6 °C under a solar intensity of 800 W m^{-2} and convective heat transfer coefficient (h) of 12 W m^{-2} K^{-1}.[2] Further, the fabrication of SiO_2 photonic crystals on Si substrates using photolithographic patterning and dry-etching processes was experimentally demonstrated to achieve up to 13 °C reduction in temperature rise of Si wafers under a solar intensity of 500–1000 W m^{-2} in Stanford, California, USA. For scalable production, a 50 μm thick layer of metamaterials was fabricated by randomly distributing 6 vol.% SiO_2 microspheres within polymethylpentene polymers to achieve translucent properties with an average light emissivity of >93 % in the atmospheric window.[14,18] Similarly, adding 6 vol.% of SiO_2 microspheres with a diameter of 4 μm to acrylic resin provided a visible light transmission of ≈91 % and an average light emissivity of >93 % in the atmospheric window.[1] However, these demonstrations of transparent radiative cooling require sophisticated and expensive fabrication processes, or further improvements in the performance of radiative cooling with high mechanical flexibility while overcoming translucence are required for more ubiquitous applications. For instance, in a transparent radiative cooling platform, SiO_2 microspheres play an important role in light emission in the atmospheric window; however, even when a small quantity of SiO_2 microspheres is added to a flexible and transparent matrix, it results in visibly opaque outputs owing to the increased random light scattering. The ideal, visibly clear daytime radiative cooler is to transmit the most visible light, to reflect near-infrared (NIR), and to radiate heat in the atmospheric window. Diverse strategies have been demonstrated to reflect NIR (0.74–2.5 μm) region, while transmitting visible light and radiating heat in the atmospheric window.[21,22] Albeit the significant progress, reflecting NIR region accompanies the considerable sacrifice of the visible light transmission and/or the heat emission in the atmospheric window. Herein, we demonstrate the synthesis of visibly clear and flexible radiative cooling metamaterials by employing an optical modulator (n-hexadecane)-infiltrated SiO_2 aerogel microparticles in a silicone elastomer (e.g., PDMS). The use of the optical modulator remarkably suppresses visible light scattering, thereby achieving a light transmission of >91 % (average haze factor of ≈0.25) for visible light and >98 % light emission in the atmospheric window. The radiative cooling performance of the visibly clear metamaterials was experimentally characterized with Si solar cells, resulting in temperature drops of ≈9 and ≈8 °C for indoor (solar intensity of 1000 W m^{-2}) and outdoor conditions (solar intensity of ≈920 W m^{-2} in Seoul, South Korea), respectively. The performance of the metamaterials synthesized in this study was also verified with commercial solar cells, which suppressed the degradation of solar light energy conversion efficiencies by 9.5 % under heat generation, compared to control solar cells without metamaterials. Furthermore, it was observed that the metamaterial glass mitigated the rise in the temperature of indoor air by ≈3.6 °C.

2. Results and Discussion

2.1. Fabrication of a Visibly Clear Radiative Cooling Metamaterial

Figure 1a schematically illustrates the visibly clear radiative cooling metamaterial synthesized in this study and its working principle. The metamaterial consists of SiO_2 aerogel microparticles infiltrated with an optical modulator (n-hexadecane) and randomly distributed in a silicone elastomer (PDMS). SiO_2 is known to effectively emit light at approximately 9.7 μm by the phonon-polariton resonance of Si—O bonds,[13,14,23] and shaping SiO_2 into microspheres can enhance the light emission in the atmospheric window by inducing Mie scattering.[15,23] A wide range of diameters of microspheres are preferred to broaden their absorption bands at the expense of decreased peak intensities because the extinction coefficients of microspheres change according to their size.[14,19,23] However, small amounts of randomly distributed SiO_2 microspheres in the silicone elastomer act as non-absorbing scatterers of visible light, rendering the photonic coolers visibly translucent. Hence, we employed 2–25 μm-sized SiO_2 aerogel microparticles constructed by an irregular connection of ≈20 nm-sized nanospheres that were fully infiltrated and covered with n-hexadecane to synthesize visibly clear metamaterials. PDMS, SiO_2, and n-hexadecane have similar refractive indices and low extinction coefficients at visible wavelengths,[24–27] and PDMS and n-hexadecane are compatible in terms of solubility[28,29] (Figure S1 and Table S1, Supporting Information).[24,27,29–34] Importantly, n-hexadecane has a comparable surface energy (27.5 mN m^{-1}) and low viscosity (0.0345 g cm^{-1} s^{-1}) relative to PDMS (surface energy of 19.8 mN m^{-1} and viscosity of 51 g cm^{-1} s^{-1}),[35–38] which enables the effective infiltration of n-hexadecane into small pores within the SiO_2 aerogel microparticles. Complete infiltration of n-hexadecane into SiO_2 aerogel microparticles produces equivalent effects such that the nanospheres are arranged to form a microstructural shape in PDMS. The resulting outcome is remarkable in that they act as an effective photonic cooler while significantly suppressing visible light scattering, as shown in Figure 1b,e. The synthesized visibly clear metamaterials are not only readily scalable but also have high mechanical flexibility,

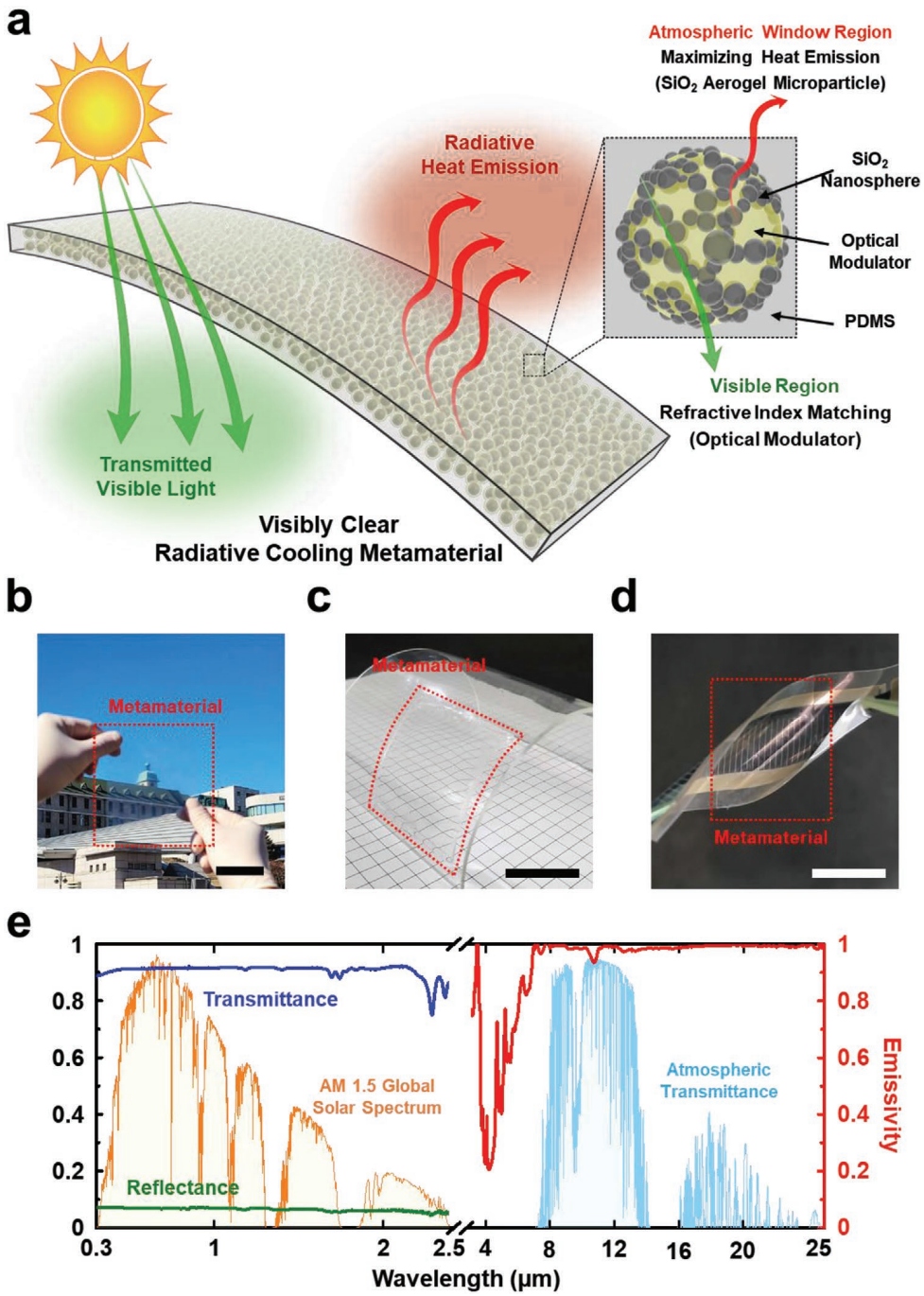

Figure 1. Visibly clear radiative cooling metamaterials. a) Schematic illustration and working principle. An optical modulator infiltrated into SiO_2 aerogel microparticles suppresses visible light scattering, thereby leading to a much higher loading of SiO_2 aerogel microparticles in a silicone elastomer while maintaining visible clarity of metamaterials. Photographs showing the metamaterials with b) visible clarity, and mechanical flexibilities attached c) on a curved glass and d) on a flexible organic solar cell. e) Measured transmittance (blue curve) and reflectance (green curve) in the AM 1.5 Global (1.5G) solar spectrum and emissivity (red curve) in the atmospheric transmittance window of the 150 μm-thick metamaterial. Scale bars: (b), (c), and (d) 2 cm.

enabling the attachment of the metamaterials to a curved window (Figure 1c) and a flexible solar cell (Figure 1d). It should be noted that although n-hexadecane has a freezing point of ≈18 °C, the solidification of n-hexadecane in metamaterials brings about no distinct change in visible clarity (Figure S2, Supporting Information).

2.2. Study of the Mechanism of Realizing Visible Clarity in Radiative Cooling Metamaterials

Figure 2a–c shows a comparison of the optical characteristics of the metamaterials synthesized in this study and control samples (i.e., SiO_2 microspheres or aerogel microparticles in

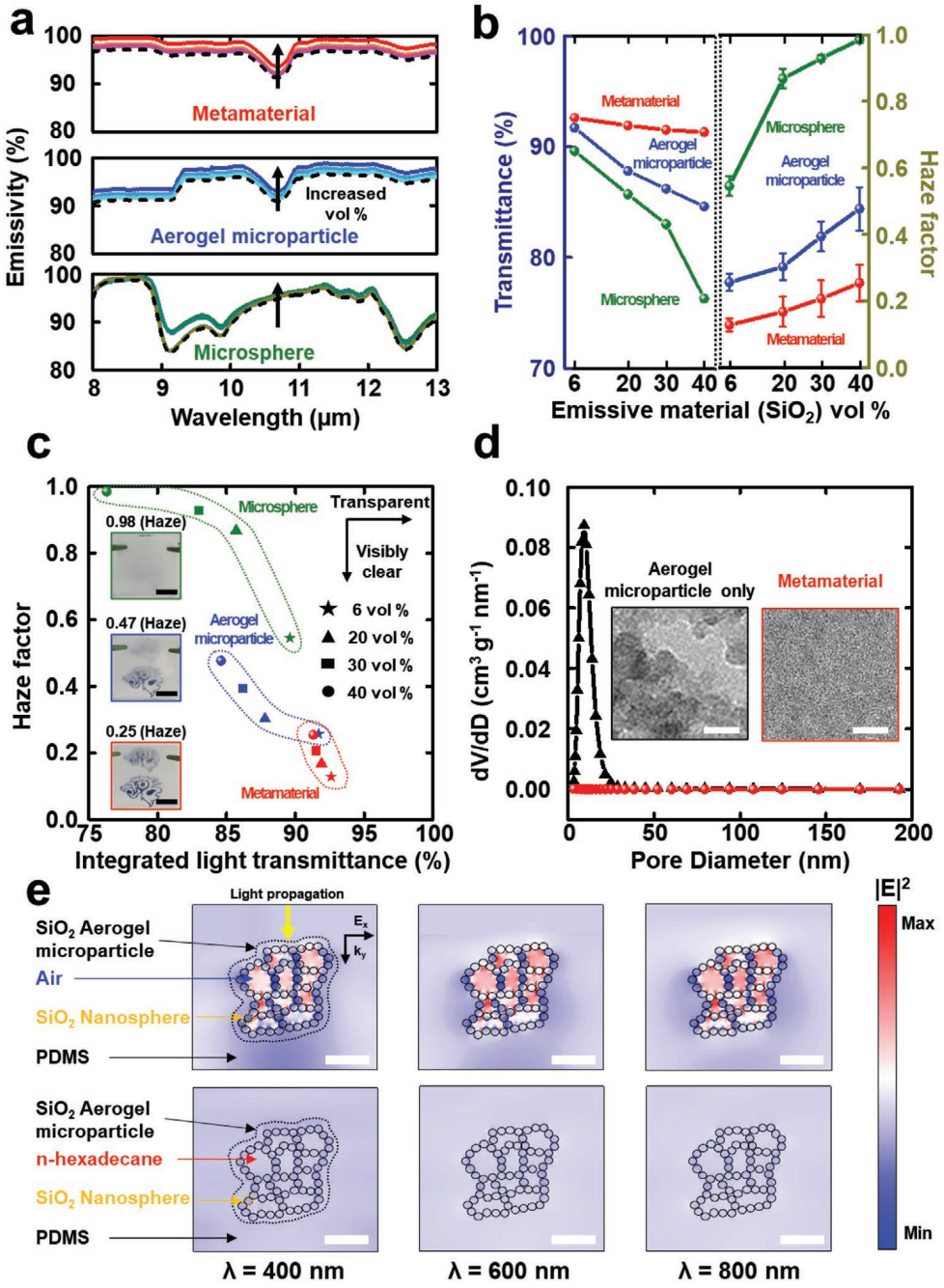

Figure 2. Mechanism to realize a visibly clear radiative cooling metamaterial. Comparisons of the measured optical characteristics of metamaterials and control samples (SiO_2 microspheres and SiO_2 aerogel microparticles in PDMS) in terms of 6, 20, 30, and 40 vol% SiO_2 contents (the volume fraction before mixing is used). a) Emissivity at the atmospheric window (wavelengths of 8–13 μm), b) integrated light transmittance and average haze factor at wavelengths of 400–800 nm, and c) average haze factors versus integrated light transmittance of the metamaterial synthesized in this study and control samples. d) Representative pore size distributions and TEM images (inset) of SiO_2 aerogel microparticles and metamaterials. e) Simulated electric fields of simplified 2D models without (top) and with n-hexadecane infiltration (bottom) at wavelengths of 400, 600, and 800 nm. Scale bars: (c) 1 cm (inset); (d) 20 nm (inset); (e) 100 nm.

PDMS without an optical modulator) with an identical thickness of 150 μm (Figures S3–S6, Supporting Information). It should be noted that the SiO_2 volume fraction of the metamaterials is based on the material fractions before mixing. Although the integrated emissivity in the atmospheric window increases slightly, adding SiO_2 contents above 6 vol.% do not distinctly increase the emissivity, as shown in a previous study.[1] Importantly, the haze factor of 6 vol.% SiO_2 microspheres is 0.55 with a considerably reduced visible clarity. The previous studies with the randomized glass-polymer hybrid focused on the random distribution of SiO_2 microspheres in a polymer matrix to maximize heat emission in

the atmospheric window, which also lead to scattering visible light.[14,23,39] To realize sub-ambient daytime radiative cooling, additional layer/structures were equipped to the polymer matrix for maximizing a visible light reflectance, thereby achieving a solar reflectance of 0.94–0.97 and an atmospheric window emissivity of 0.90–0.96. However, the metamaterials synthesized by us successfully suppressed the loss of visible clarity owing to the existence of an optical modulator. The visibly clear metamaterials with an inclusion of ≈40 vol.% SiO_2 aerogel microparticles achieved an integrated light emission of >98 % in the atmospheric window with a visible light transmission of >91 % and haze factor of 0.2–0.32 (an average of 0.25) at wavelengths of 400–800 nm. SiO_2 aerogel microparticles in PDMS exhibited a slightly higher light emission than SiO_2 microspheres in the atmospheric window because of the favorable size distribution[14,23] of the SiO_2 aerogel microparticles (2–25 μm) compared to the SiO_2 microspheres (≈4 μm) and the pore-driven multiple diffuse reflections[15,40] of the aerogel microparticles. The visible light transmission of the SiO_2 aerogel microparticles was higher than that of the microspheres, which was distinguishable in the higher volume fraction, presumably due to the partial infiltration of PDMS in the aerogel microparticles (Figure S7, Supporting Information). The enhanced light emission of metamaterials compared to that of SiO_2 aerogel microparticles in the atmospheric window can be attributed to the C—C and C—H bonds of n-hexadecane, which are favorable for increasing light emission at wavelengths of 3–4 and 7–15 μm.[15] Therefore, the SiO_2 aerogel microparticles infiltrated with n-hexadecane provide an effective resonant platform in the atmospheric window. As the metamaterial thickness increases from 30 to 3000 μm, the integrated emissivity of the metamaterial in the atmospheric window increases from 95.6 % to 98.9 %, but it sacrifices visibly clarity (Figure S8, Supporting Information). We further compared the pore distributions and transmission electron microscopy (TEM) images of the metamaterials with those of SiO_2 aerogel microparticles, as shown in Figure 2d. The absence of a distinct peak in the pore distributions and the color contrasts in the TEM images of the metamaterials clearly indicate the full infiltration of n-hexadecane into the SiO_2 aerogel microparticles in the metamaterials. The complete infiltration of an optical modulator not only ensures matching of refractive indices among the contents of metamaterials by replacing air with n-hexadecane but also suppresses visible light scattering induced by SiO_2 aerogel microparticles, as shown in the finite-difference time-domain (FDTD) simulation (Figure 2e). When a plane wave with wavelengths of 400, 600, and 800 nm is incident on the metamaterials, the n-hexadecane within the SiO_2 aerogel microparticles can effectively transmit the incident visible light with minimal scattering because of the similar refractive indices of PDMS, SiO_2, and n-hexadecane, while the air within the aerogel microparticles induces significant visible light scattering. However, the material of the optical modulator is not limited to n-hexadecane. When using oil with similar optical properties and solubility (e.g., silicone oil), visibly clear radiative cooling characteristics can be achieved, and the slippery surface properties can also be imparted to the metamaterials (Figure S9, Supporting Information).

2.3. Temperature Monitoring in Indoor and Outdoor Conditions

To quantify the radiative cooling performance of visibly clear metamaterials, the temperature was monitored both in indoor and outdoor conditions, as shown in **Figure 3**. Specifically, we carried out real-time measurements of the surface temperatures of Si solar cells positioned in the middle of a wooden frame, which was covered by an aluminum foil to reflect the incident solar light and prevent unwanted heat gain from the wooden frame. Additionally, a low-density polyethylene (LDPE) film transparent in the visible and infrared light region was used to cover the wooden frame, thus acting as a windshield and suppressing the convective heat transfer to investigate the effects of radiative heat transfer only. Non-radiative heat exchange coefficients for indoor and outdoor conditions were obtained as 3.0–4.8 and 3.1–5.0 W m^{-2} K^{-1}, respectively. For measurements in indoor conditions, the LDPE-covered wooden frame apparatus was illuminated by an AM 1.5 Global (1.5G) solar simulator at ≈26 °C and a relative humidity of ≈30 % (Figure 3a,b). While continuous and intensive solar light illumination (1000 W m^{-2}) by the solar simulator inevitably increases the surface temperatures of Si solar cells, placing our visibly clear metamaterials on top of Si solar cells (58.1 °C) considerably suppressed the rise in temperature by 8.5 °C at 100 min after illumination compared to the control Si solar cells without metamaterials (66.6 °C), as shown in Figure 3c. The significant reduction in temperature rise shows effective light emission in the atmospheric window of the metamaterials synthesized by us. Placing the metamaterial on a solar cell leads to the significant decrease of the heating rate of solar cells by 17.3–21.0%: the bare solar cell reaches the stable temperature under AM 1.5G solar illumination with the temperature rise of 37.4–39.8 °C in 50–70 min (0.57–0.75 °C min^{-1}), while the metamaterial-covered solar cell approaches the stable temperature with the temperature rise of 30.9–31.3 °C in 50–70 min (0.45–0.62 °C min^{-1}). Based on our experiments, when placing the metamaterials on a solar cell, the time to reach the near-steady-state condition is also slightly shorter or comparable to the control sample. We also investigate the cooling performance of metamaterials, compared with a conventional thermal emitter (e.g., thick planar PDMS layer) in Figure S10, Supporting Information. The integrated emissivity of 30–3000 μm thick PDMS layer in the atmospheric window ranges between 81–93 %, while the 30–3000 μm thick metamaterials exhibit the integrated emissivity of 95–99 %. For indoor, the suppression of the temperature rise in the PDMS-covered solar cell and the metamaterial-covered solar cells is 1.9–6.4 and 2.8–9.1 °C, respectively. Increasing the film thickness can increase the integrated emissivity, while accompanying the increased conductive thermal resistance.[41] As such, the 150 μm thick PDMS-covered solar cells exhibit 6.4 °C suppression of the rise in temperature, while 30 μm thick metamaterial-covered solar cells exhibit 9.1 °C suppression of the rise in temperature under AM 1.5G solar illumination for 100 min. The radiative cooling characteristics of the transparent metamaterials were further investigated under outdoor conditions, specifically, clear sky conditions in Seoul, South Korea. As shown in Figure 3d, two LDPE-covered wooden frame apparatuses were built to simultaneously monitor the radiative cooling performance of Si solar cells with and without metamaterials; however, they

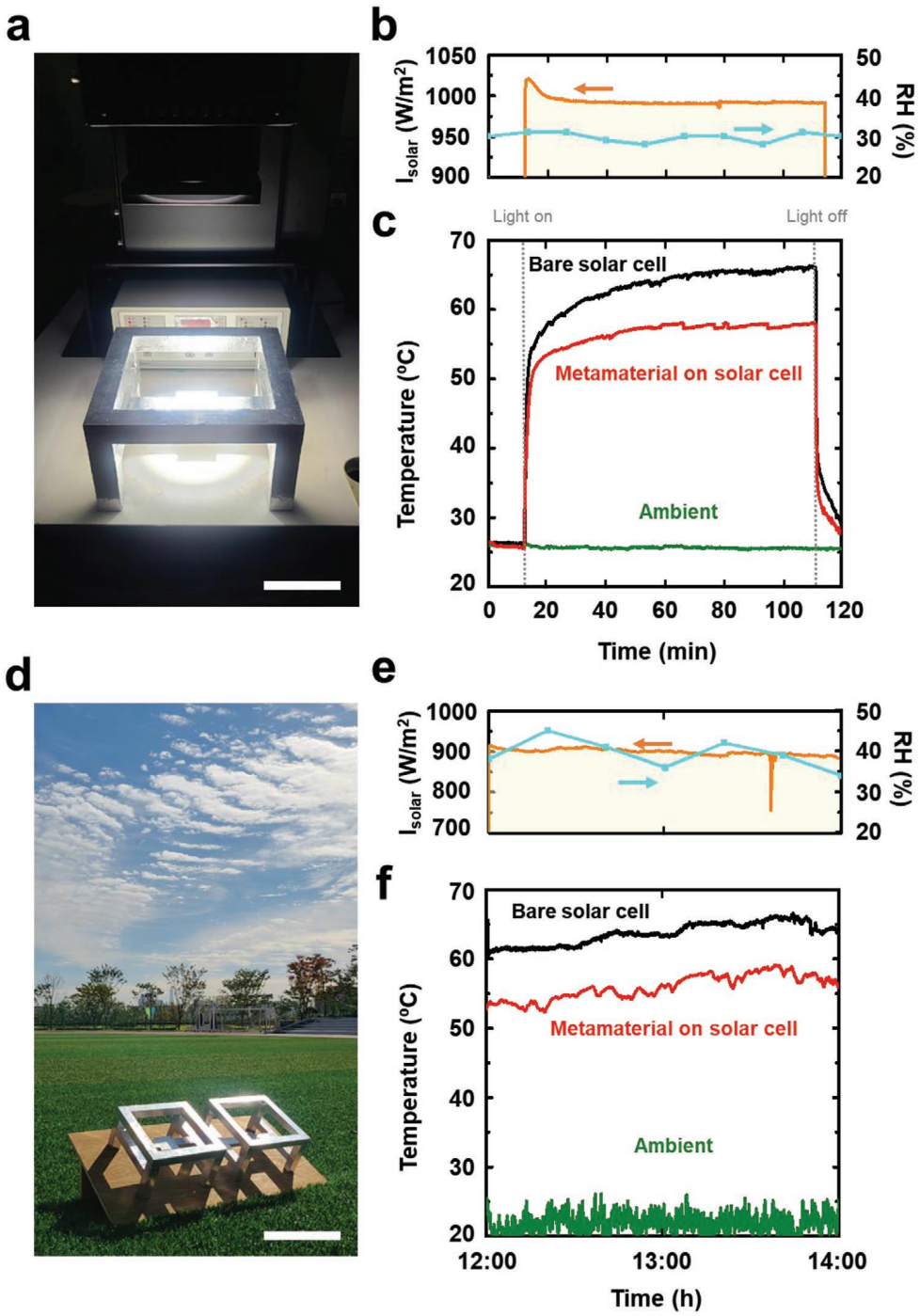

Figure 3. Temperature monitoring of visibly clear radiative cooling metamaterials placed on top of commercial Si solar cells in a–c) indoor and d–f) outdoor conditions. Indoor and outdoor daytime radiative cooling performance of the metamaterial. (a,d) Photograph, (b,e) solar intensity (I_{solar}), relative humidity (RH), and (c,f) variations in ambient temperature (green curve), metamaterial on a solar cell (red curve), and a control bare solar cell (black curve) in indoor conditions under illumination by an AM 1.5G solar simulator and in outdoor conditions under solar irradiation in Seoul, South Korea. Scale bars: (a) 10 cm; (d) 25 cm.

were tilted 30° toward the south to maximize solar irradiance such that sunlight is near-normally incident on the samples around noon. Figure 3e indicates the measured solar intensity of ≈920 W m^{-2}, ambient temperature of 20–25 °C, and relative humidity of 30–45% during the outdoor measurements. The visibly clear metamaterials synthesized in this study exhibit distinct radiative cooling characteristics by suppressing the temperature rise of Si solar cells by an average of 7.7 °C (5–12 °C). We theoretically estimate the net cooling power in terms of metamaterial surface temperatures and combined non-radiative heat exchange coefficients (Figure S11, Supporting Information). For the difference between ambient temperature and

metamaterial surface temperature as −6 °C, the estimated net cooling power is 113–149 W m^{-2} in the range of combined non-radiative heat exchange coefficients from 0 to 6 W m^{-2} K^{-1}. Notably, high humidity decreases the radiative cooling performance owing to re-emission by atmospheric radiation.[42] At a higher humidity (46–60%) with similar solar intensities and ambient temperatures, the visibly clear metamaterial can still reduce the temperature rise of Si solar cells by an average of 6.7 °C (5–8 °C) (Figure S12, Supporting Information). To the best of our knowledge, our visibly clear metamaterials exhibit the highest transparent radiative cooling effects in environments similar to the reported humidity range of 30–60%. Despite the efforts to avoid electrical interferences among thermocouples during the simultaneous measurements on bare and metamaterial-covered solar cells, temperature fluctuations in Figure 3f may still result from the irregular, gentle wind blowing over the data acquisition computer placed outside the cooling apparatus. The temperature fluctuations in Figure 3c and Figure S12, Supporting Information, are mitigated under the identical measurement setup. Therefore, the temperature fluctuations minimally affect the results such that placing a visible clear radiative cooler on the solar cells significantly reduces the temperature rise under solar irradiance.

2.4. Metamaterial-Integrated Solar Cells and Window Glasses

Heat generation of solar cells degrades the solar energy conversion efficiencies by decreasing the open-circuit voltages and fill factors in spite of a slight increase in short-circuit current densities.[43] To determine the potency of the visibly clear radiative cooling metamaterials, the variation in the performance of commercial Si solar cells covered with metamaterials was investigated on light soaking using an AM 1.5G solar simulator (**Figure 4**a). The commercial glass-covered Si solar cell module has six Si solar cells connected in series. A single Si solar cell has a width of 7.8 cm and a length of 2 cm. Figure 4b shows the solar cell characteristics of the modules with and without the transparent metamaterial. Compared to the control solar cell module (efficiency of 10.35 %, open-circuit voltage of 3.65 V, short-circuit current density of 27.69 mA cm^{-2}, and fill factor of 0.61), slightly higher solar energy conversion efficiencies were achieved by placing metamaterials on the top (efficiency of 11.26 %, open-circuit voltage of 3.69 V, short-circuit current density of 29.32 mA cm^{-2}, and fill factor of 0.62). The J-V curves of the solar cells with and without metamaterials in Figure 4b were measured at the identical solar cell temperature (≈25 °C) and the integrated light absorption of solar cells with and without metamaterials is 82.5 % and 75.1 % in wavelengths from 400 to 800 nm (Figure S13, Supporting Information). Therefore, the increased solar energy conversion efficiencies with metamaterials in Figure 4b can be attributed to the anti-reflection effects of the latter owing to the graded refractive index. It should be noted that the metamaterial thickness considered in this study is not optimized to maximize the anti-reflection effects. Importantly, the metamaterials in this study distinctly suppressed the performance degradation of solar cells when light-soaked using the AM 1.5G solar simulator for 100 min. Figure 4c shows the temperature and normalized efficiency (i.e., the efficiency normalized by the initial efficiency) of the solar cell modules in terms of the light-soaking time. While the temperature of Si solar cells increases due to light soaking, the metamaterial-covered Si solar cell module (normalized efficiency reduction of 17%) exhibits 1.5 times lower degradation than the control Si solar cell module (normalized efficiency reduction of 26 %) due to the effective heat emission and suppressing of the temperature rise of the solar cells by approximately 8.5 °C out of the total 40.6 °C. Finally, we demonstrated a visibly clear radiative cooling window platform employing our synthesized metamaterials, which is the first of its kind (Figure 4d and Figure S14, Supporting Information). Specifically, the metamaterial glass was prepared by integrating a 150 μm-thick visibly clear metamaterial film between transparent glass (i.e., potassium bromide (KBr)) at wavelengths of 0.25–26 μm and soda-lime glass using an adhesive layer (polydimethylsiloxane). Figure 4e and Figure S15, Supporting Information, show the temperature variation for the glass in the LDPE-covered wooden frame apparatus upon exposure to AM 1.5G solar illumination at an ambient temperature of 18 °C and a relative humidity of ≈30% for 100 min. It should be noted that the total thicknesses of the bare soda-lime glass and metamaterial glass are almost the same (≈6.2 mm). While the temperature of the bottom plane of bare soda-lime glass increases to 38.9 °C, the metamaterial glass exhibits significant cooling effects of approximately 3.9 °C. In addition, the temperature of the indoor air underneath the metamaterial glass with a gap of 5 mm was also confirmed to have a cooling effect of 3.6 °C compared to bare glass. The lower temperature difference compared to the solar cell experiments is attributed to the absence of intense light-absorbing materials under the glass. Nonetheless, the significant cooling effects of the metamaterial glass indicate its potential as a visibly clear radiative cooling window for building and automobile applications.

3. Conclusion

In this study, we demonstrated the synthesis of visibly clear radiative cooling metamaterials using a rational design to deploy an optical modulator (n-hexadecane) in SiO_2 aerogel microparticles within a silicone elastomer matrix. While the random distribution of large amounts (40 vol.%) of SiO_2 aerogel microparticles with fully infiltrated n-hexadecane contributes to an integrated emissivity of >98 % in the atmospheric window, the visible light scattering is simultaneously suppressed to achieve visible light transmission of >91 % at wavelengths of 400–800 nm. The visibly clear metamaterials can be readily fabricated in a reproducible and scalable manner owing to the facile synthesis method based on the random distribution of particles. The indoor temperature measurements performed on solar cells confirmed the excellent cooling characteristics of the metamaterials synthesized by us to suppress the temperature rise of the solar cells by 8.5 °C under AM 1.5G light illumination. In addition, outdoor temperature measurements were performed on solar cells in the autumn sky of Seoul, South Korea (solar intensity of ≈920 W m^{-2} and relative humidity of 30–45 %), indicating the effective cooling capability of our metamaterial with considerable suppression of the temperature rise of the solar

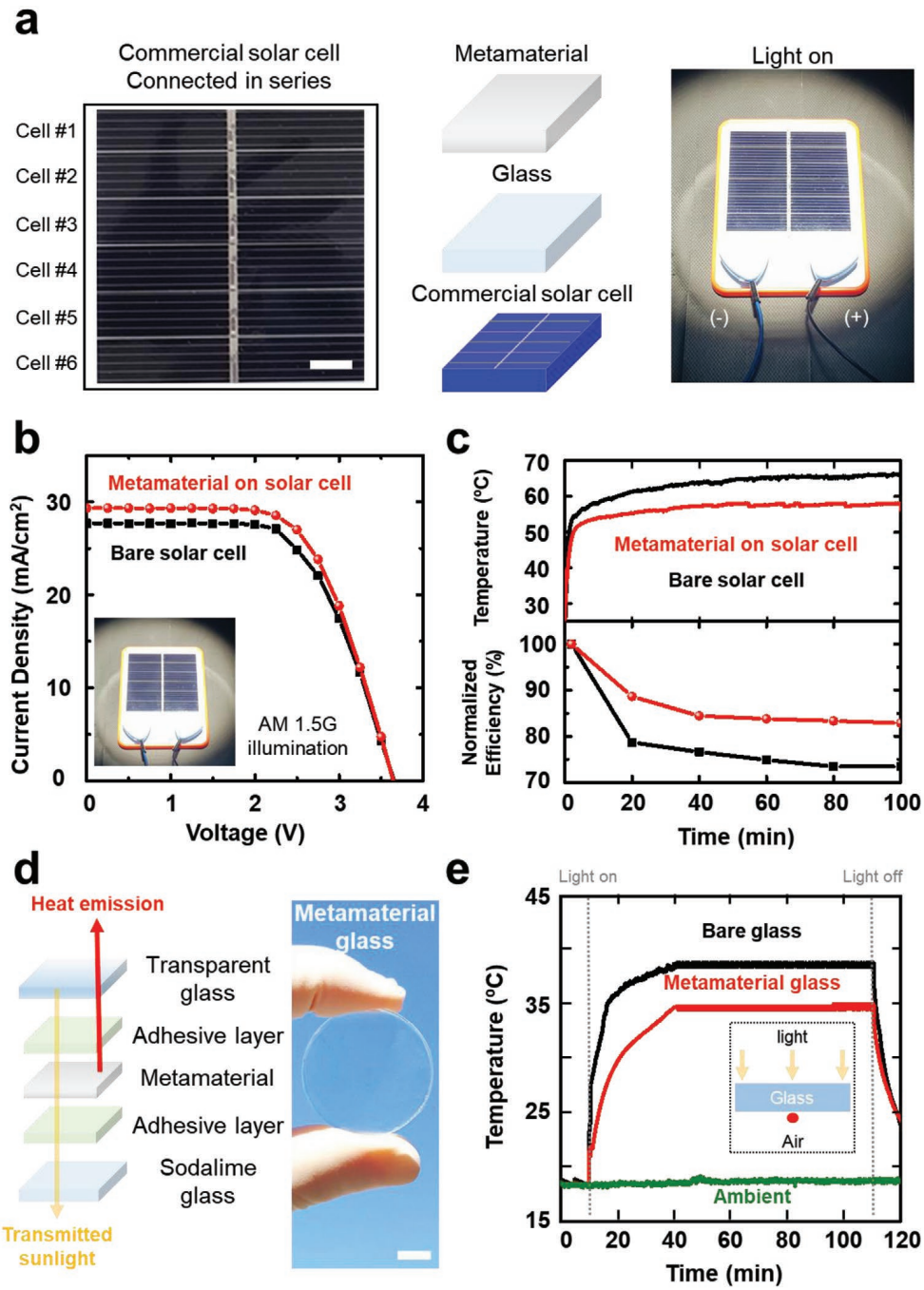

Figure 4. Metamaterial-integrated solar cells and window glasses. a) Metamaterial-integrated solar cells: photographs of (left) top and (right) perspective views, and (middle) schematics in an expanded view to illustrate that the metamaterial is placed on top of the glass layer of a commercial Si solar cell module. b) Measured current density and voltage curves of the commercial solar cell modules with and without metamaterials under AM 1.5G illumination. c) Temperature and normalized efficiency of the commercial solar cell modules with and without metamaterials under light-soaking tests by a solar simulator. d) Schematic (left) and photograph (right) of the fabricated metamaterial glass. e) Variations in the ambient temperature (green curve) and the bottom planes of the metamaterial glass (red curve) and bare soda-lime glass (black curve) in indoor conditions under AM 1.5G illumination. Scale bars: (a) and (d) 1 cm.

cells by an average of 7.7 °C (5–12 °C). We further demonstrated the distinct advantages of employing these visibly clear radiative cooling metamaterials in solar cells and windows. Placement of the metamaterial on top of commercial Si solar cell modules not only increased their initial performance but also helped in achieving a lower thermal degradation by 1.5 times at 100 min after light soaking. Additionally, it was observed that visibly clear metamaterial glass can suppress the temperature rise of general soda-lime glass by 3.9 °C in light-soaking tests. Adding the reflection functionality of NIR region to the

metamaterials should be further investigated to realize an ideal, visibly clear daytime radiative cooler. Our work paves the way for wide applications of photonic radiative cooling technology with high performance and large-scale production for efficient renewable power generation and enhanced energy saving.

4. Experimental Section

Fabrication and Characterization of Visibly Clear Radiative Cooling Metamaterial: The silicone elastomer (PDMS) solution was prepared by mixing a silicone elastomer and curing agent (Sylgard 184, Dow Corning) at a weight ratio of 10:1, and a mixture of SiO_2 aerogel microparticles (2–25 μm in size, Sigma-Aldrich) and n-hexadecane (Sigma-Aldrich) was prepared with a volume ratio of 2:1. Visibly clear radiative cooling metamaterials were fabricated by mixing the silicone elastomer solution, SiO_2 aerogel microparticles, and n-hexadecane in a volume ratio of 4:4:2 (the volume fraction before mixing was indicated) using a centrifugal mixer (ARE-310, Thinky) at 2000 rpm for 3 min, followed by heating at 100 °C for 2 h. It should be noted that the volume ratios of SiO_2 aerogel microparticles and n-hexadecane were optimized for proper mixing (Figure S6, Supporting Information). As a control sample for comparison with metamaterials, films were prepared by mixing SiO_2 microspheres (4 μm in size, Figure S3, Supporting Information) or SiO_2 aerogel microparticles (Figure S4, Supporting Information) with PDMS according to the volume fractions. Cross-sectional TEM images were obtained by freezing the metamaterial mounted on a cryo-pin by flowing liquid nitrogen. The metamaterial with a thickness of 100 nm was prepared using a cryo-ultramicrotome (CR-X, RMC Boeckeler). Pore distributions were characterized using the Barrett–Joyner–Halenda (BJH) method (TriStar II 3020, Micromeritics). The light transmission and reflectance of the metamaterials were measured at wavelengths of 300–2500 nm and 3–15 μm using a UV-visible spectrometer equipped with an integrating sphere (Lambda 650S, Perkin Elmer) and a Fourier transform infrared spectrometer (Nicolet 6700, Thermo Scientific), respectively. Optical characterization was performed using an identical film with a thickness of 150 μm.

Fabrication of Metamaterial Glass: Metamaterial glass was fabricated to simulate a visibly clear radiative cooling glass. The metamaterial was inserted between a transparent glass at wavelengths of 0.25–26 μm (KBr, Edmund Optics) and a commercial soda-lime glass, with a thickness of 3 mm each. Specifically, liquid-state PDMS was spin-coated on a soda-lime glass at 2000 rpm for 2 min after which a 150 μm-thick metamaterial film was attached to it. Then, the liquid-state PDMS was again spin-coated over the metamaterial film at 2000 rpm for 2 min. The transparent glass was then attached on top of the liquid-state PDMS. Finally, the metamaterial glass was cured at 150 °C for 10 h under vacuum conditions, and a pressure of 4 kPa was applied to the glass. The fabricated metamaterial glass had a thickness of ≈6.2 mm.

FDTD Numerical Simulation: FDTD simulations of the metamaterial were performed using commercial FDTD software (Lumerical Solutions). To qualitatively investigate the influence of n-hexadecane and SiO_2 aerogel microparticles in a PDMS layer, a single unit cell of the 2D model with periodic boundary conditions on the sides and a perfectly matched layer boundary condition at the bottom was set. A plane wave source at wavelengths ranging between 400–800 nm was positioned at a distance of 250 nm from the top surface of the PDMS. The refractive indices of PDMS, n-hexadecane, and SiO_2 were set as 1.43, 1.43, and 1.46, respectively. Light propagation through the unit cell was monitored and quantified by calculating the light intensity.

Measurement of Indoor Temperature and Photovoltaic Properties: To quantitatively determine the cooling capability of the metamaterials, the temperatures of the samples in the wooden frame ($25 \times 25 \times 15$ cm^3) covered by an aluminum foil and illuminated by an AM 1.5G solar simulator (Oriel Sol3A, 94023A, Newport) were measured. The apparatus was placed horizontally for normal illumination of the solar beam onto the sample surfaces. An optically transparent LDPE film was used as a windshield to cover the top of the apparatus. A bare silicon solar cell (area of 7.8×2 cm^2) was used as a sample to measure the temperature. The temperature and humidity were measured using type T thermocouples and a hygrometer, respectively. The current-voltage characteristics of commercial Si solar cells were measured with a glass top under illumination by an AM 1.5G solar simulator. The voltage step was 10 mV, and the current density was calculated by dividing the measured current by the full device area of 93.6 cm^2. The photovoltaic properties were measured five times for each device. The light-soaking tests were conducted for 100 min and the corresponding photovoltaic properties were characterized every 20 min.

Outdoor Temperature Measurement: The outdoor temperature measurements were carried out on metamaterials using the apparatus in which a wooden frame ($25 \times 25 \times 15$ cm^3) was covered with an aluminum foil and wind-shielded by an LDPE film on a flat surface at Hanyang University, Seoul, South Korea in mid-September 2020. The peak elevation of the sun was 50–60° above the horizon on the days when measurements were taken, whereas the apparatus was tilted 30° toward the south such that the sunlight illuminated near-normally on the sample at the maximum solar irradiance. To compare the temperature of the silicon solar cell based on the usage of metamaterials in the same environment, a bare silicon solar cell (area of 7.8×2 cm^2) and that with a metamaterial (area of 7.8×2 cm^2) were placed in each apparatus, fixed to the tilted frame, and the temperature on the surface was measured. The temperature was measured using type T thermocouples, and solar irradiance was monitored using a pyranometer (SR15, Jinyoung Tech). The humidity was measured using a hygrometer.

Non-Radiative Heat Exchange Coefficients Estimation: Radiation domes were constructed by covering the measurement apparatus with aluminum foil to block radiative heat exchange.[44] After monitoring the transient temperatures of silicon substrate or soda lime glass placed on the illumination zone in the radiation dome, the non-radiative heat exchange coefficients of the samples (the measurement apparatus) were estimated by using the well-known lumped parameter model. As a result, the non-radiative heat exchange coefficients in indoor and outdoor conditions were 3.0–4.8 and 3.1–5.0 W m^{-2} K^{-1}, respectively.

Net Cooling Power Estimation: The net cooling power (P_{net}) of the radiation power from metamaterial (P_{rad}), the thermal power from solar irradiance (P_{sun}), the absorbed power due to surrounding atmospheric radiation (P_{atm}), and the cooling power due to non-radiative heat exchange ($P_{cond+conv}$) in terms of cooler surface temperature (T) and ambient temperature (T_{amb}) can be expressed as follows:[18]

$$P_{net}(T) = P_{rad}(T) - P_{atm}(T_{amb}) - P_{sun} + P_{cond+conv}(T, T_{amb}) \quad (1)$$

In the visibly clear radiative cooling metamaterials synthesized, the ambient temperature was lower than the operating temperature of the metamaterials ($T_{amb} < T$). The radiation power from metamaterial (P_{rad}) is expressed as follows:[18,45]

$$P_{rad}(T) = 2\pi \int_0^{\pi/2} \int_0^{\infty} I_{BB}(T,\lambda)\varepsilon_r(\lambda,\theta)\sin(\theta)\cos(\theta)\,d\lambda\,d\theta \quad (2)$$

where I_{BB} is the spectral radiance of a blackbody at temperature T in the range of 8–13 μm, ε_r is the emissivity of metamaterial, and θ is the zenith angle. It was assumed that the metamaterial normally faces the sun,[45] which makes the zenith angle as 0 deg. The cooling power due to non-radiative heat exchanger ($P_{cond+conv}$) is expressed as follows:[18]

$$P_{cond+conv} = h_c A(T - T_{amb}) \quad (3)$$

where A is the exposed surface area of metamaterial and h_c is a combined non-radiative heat transfer coefficient. The light absorption by the metamaterial was ≈2 % in the AM1.5G solar spectrum between wavelengths from 300 nm to 2.5 μm, resulting in P_{sun} as 20 W m^{-2}.

Assuming T_{amb} as 25 °C, P_{atm} (T_{amb}) was estimated as 29 W m^{-2} in the atmospheric window (wavelengths of 8–13 μm).

Supporting Information

Supporting Information is available from the Wiley Online Library or from the author.

Acknowledgements

This project was supported by the Basic Science Research Program (NRF-2021R1A2C1011418) through the National Research Foundation of Korea (NRF) funded by the Ministry of Science and ICT of Korea. C.H.L. acknowledges funding support from the Asian Office of Aerospace Research & Development (AOARD: FA2386-16-1- 4105; program manager: Dr. Tony Kim) and the Air Force Office of Scientific Research (AFOSR: FA2386-18-1-40171; program manager: Dr. Tony Kim). C.H.L. also acknowledges the Leslie A. Geddes Endowment at Purdue University.

Conflict of Interest

The authors declare no conflict of interest.

Data Availability Statement

Research data are not shared.

Keywords

aerogels, metamaterials, photonic coolers, radiative cooling, transparent metamaterials

Received: June 17, 2021
Revised: September 17, 2021
Published online:

[1] C. Ziming, W. Fuqiang, G. Dayang, L. Huaxu, S. Yong, *Sol. Energy Mater. Sol. Cells* **2020**, *213*, 110563.
[2] L. Zhu, A. Raman, K. X. Wang, M. A. Anoma, S. Fan, *Optica* **2014**, *1*, 32.
[3] T. Li, Y. Zhai, S. He, W. Gan, Z. Wei, M. Heidarinejad, D. Dalgo, R. Mi, X. Zhao, J. Song, J. Dai, C. Chen, A. Aili, A. Vellore, A. Martini, R. Yang, J. Srebric, X. Yin, L. Hu, *Science* **2019**, *364*, 760.
[4] P. C. Hsu, C. Liu, A. Y. Song, Z. Zhang, Y. Peng, J. Xie, K. Liu, C. L. Wu, P. B. Catrysse, L. Cai, S. Zhai, A. Majumdar, S. Fan, Y. Cui, *Sci. Adv.* **2017**, *3*, e1700895.
[5] Y. Peng, J. Chen, A. Y. Song, P. B. Catrysse, P. C. Hsu, L. Cai, B. Liu, Y. Zhu, G. Zhou, D. S. Wu, H. R. Lee, S. Fan, Y. Cui, *Nat. Sustain.* **2018**, *1*, 105.
[6] A. P. Raman, M. A. Anoma, L. Zhu, E. Rephaeli, S. Fan, *Nature* **2014**, *515*, 540.
[7] H. Zhang, K. C. S. Ly, X. Liu, Z. Chen, M. Yan, Z. Wu, X. Wang, Y. Zheng, H. Zhou, T. Fan, *Proc. Natl. Acad. Sci. USA* **2020**, *117*, 14657.
[8] S. Y. Jeong, C. Y. Tso, Y. M. Wong, C. Y. H. Chao, B. Huang, *Sol. Energy Mater. Sol. Cells* **2020**, *206*, 110296.
[9] A. Aili, Z. Y. Wei, Y. Z. Chen, D. L. Zhao, R. G. Yang, X. B. Yin, *Mater. Today Phys.* **2019**, *10*, 100127.
[10] P. Yang, C. Chen, Z. M. Zhang, *Sol. Energy* **2018**, *169*, 316.
[11] L. Cai, A. Y. Song, W. Li, P. C. Hsu, D. Lin, P. B. Catrysse, Y. Liu, Y. Peng, J. Chen, H. Wang, J. Xu, A. Yang, S. Fan, Y. Cui, *Adv. Mater.* **2018**, *30*, 1802152.
[12] H. Bao, C. Yan, B. Wang, X. Fang, C. Y. Zhao, X. Ruan, *Sol. Energy Mater. Sol. Cells* **2017**, *168*, 78.
[13] S. Atiganyanun, J. B. Plumley, S. J. Han, K. Hsu, J. Cytrynbaum, T. L. Peng, S. M. Han, S. E. Han, *ACS Photonics* **2018**, *5*, 1181.
[14] Y. Zhai, Y. Ma, S. N. David, D. Zhao, R. Lou, G. Tan, R. Yang, X. Yin, *Science* **2017**, *355*, 1062.
[15] J. Mandal, Y. Fu, A. C. Overvig, M. Jia, K. Sun, N. N. Shi, H. Zhou, X. Xiao, N. Yu, Y. Yang, *Science* **2018**, *362*, 315.
[16] W. Gao, Z. Lei, K. Wu, Y. Chen, *Adv. Funct. Mater.* **2021**, *31*, 2100535.
[17] D. Li, X. Liu, W. Li, Z. Lin, B. Zhu, Z. Li, J. Li, B. Li, S. Fan, J. Xie, J. Zhu, *Nat. Nanotechnol.* **2021**, *16*, 153.
[18] L. Zhu, A. P. Raman, S. Fan, *Proc. Natl. Acad. Sci. U. S. A.* **2015**, *112*, 12282.
[19] S. Gamage, E. S. H. Kang, C. Åkerlind, S. Sardar, J. Edberg, H. Kariis, T. Ederth, M. Berggren, M. P. Jonsson, *J. Mater. Chem. C* **2020**, *8*, 11687.
[20] J. Mandal, M. Jia, A. Overvig, Y. Fu, E. Che, N. Yu, Y. Yang, *Joule* **2019**, *3*, 3088.
[21] M. Kim, D. Lee, S. Son, Y. Yang, H. Lee, J. Rho, *Adv. Opt. Mater.* **2021**, *9*, 2002226.
[22] Z. Zhou, X. Wang, Y. Ma, B. Hu, J. Zhou, *Cell Rep. Phys. Sci.* **2020**, *1*, 100231.
[23] X. Wang, X. Liu, Z. Li, H. Zhang, Z. Yang, H. Zhou, T. Fan, *Adv. Funct. Mater.* **2020**, *30*, 1907562.
[24] F. Schneider, J. Draheim, R. Kamberger, U. Wallrabe, *Sens. Actuators, A* **2009**, *151*, 95.
[25] J. L. Kou, Z. Jurado, Z. Chen, S. Fan, A. J. Minnich, *ACS Photonics* **2017**, *4*, 626.
[26] C. Z. Tan, *J. Non-Cryst. Solids* **1998**, *223*, 158.
[27] N. Maeda, J. N. Israelachvili, M. M. Kohonen, *Proc. Natl. Acad. Sci. USA* **2003**, *100*, 803.
[28] J. N. Lee, C. Park, G. M. Whitesides, *Anal. Chem.* **2003**, *75*, 6544.
[29] T. Lindvig, M. L. Michelsen, G. M. Kontogeorgis, *Fluid Phase Equilib.* **2002**, *203*, 247.
[30] S. Rasappa, L. Schulte, D. Borah, H. Hulkkonen, S. Ndoni, T. Salminen, R. Senthamaraikanan, M. A. Morris, T. Niemi, *Microelectron. Eng.* **2018**, *192*, 1.
[31] M. Levin, P. Redelius, *Energy Fuels* **2008**, *22*, 3395.
[32] R. Payri, F. J. Salvador, J. Gimeno, O. Venegas, *Exp. Tech.* **2016**, *40*, 261.
[33] R. C. Smith, G. T. Smith, D. Wong, *Eye* **1990**, *4*, 230.
[34] S. A. Khodier, *Opt. Laser Technol.* **2002**, *34*, 125.
[35] N. Tian, P. Zhang, J. Zhang, *Front. Chem.* **2018**, *6*, 144.
[36] T. Klein, S. Yan, J. Cui, J. W. Magee, K. Kroenlein, M. H. Rausch, T. M. Koller, A. P. Fröba, *J. Chem. Eng. Data* **2019**, *64*, 4116.
[37] S. Vudayagiri, M. D. Junker, A. L. Skov, *Polym. J.* **2013**, *45*, 871.
[38] T. J. Hinton, A. Hudson, K. Pusch, A. Lee, A. W. Feinberg, *ACS Biomater. Sci. Eng.* **2016**, *2*, 1781.
[39] Y. Chen, B. Dang, J. Fu, C. Wang, C. Li, Q. Sun, H. Li, *Nano Lett.* **2020**, *21*, 397.
[40] Y. Chen, J. Mandal, W. Li, A. Smith-Washington, C. C. Tsai, W. Huang, S. Shrestha, N. Yu, R. P. S. Han, A. Cao, Y. Yang, *Sci. Adv.* **2020**, *6*, eaaz5413.
[41] L. Zhao, B. Bhatia, S. Yang, E. Strobach, L. A. Weinstein, T. A. Cooper, G. Chen, E. N. Wang, *ACS Nano* **2019**, *13*, 7508.
[42] M. M. Hossain, M. Gu, *Adv. Sci.* **2016**, *3*, 1500360.
[43] E. Skoplaki, J. A. Palyvos, *Sol. Energy* **2009**, *83*, 614.
[44] X. Xue, M. Qiu, Y. Li, Q. M. Zhang, S. Li, Z. Yang, C. Feng, W. Zhang, J. G. Dai, D. Lei, W. Jin, L. Xu, T. Zhang, J. Qin, H. Wang, S. Fan, *Adv. Mater.* **2020**, *32*, 1906751.
[45] J. Jaramillo-Fernandez, G. L. Whitworth, J. A. Pariente, A. Blanco, P. D. Garcia, C. Lopez, C. M. Sotomayor-Torres, *Small* **2019**, *15*, 1905290.